

The motion reverse correlation (MRC) method: A linear systems approach in the motion domain

Bart G. Borghuis*, János A. Perge, Ildikó Vajda, Richard J.A. van Wezel,
Wim A. van de Grind, Martin J.M. Lankheet

Department of Functional Neurobiology, Helmholtz Institute, Utrecht University, Padualaan 8, 3584 CH Utrecht, The Netherlands

Received 28 August 2002; received in revised form 9 November 2002; accepted 11 November 2002

Abstract

We introduce the motion reverse correlation method (MRC), a novel stimulus paradigm based on a random sequence of motion impulses. The method is tailored to investigate the spatio-temporal dynamics of motion selectivity in cells responding to moving random dot patterns. Effectiveness of the MRC method is illustrated with results obtained from recordings in both anesthetized cats and an awake, fixating macaque monkey. Motion tuning functions are computed by reverse correlating the response of single cells with a rapid sequence of displacements of a random pixel array (RPA). Significant correlations between the cell's responses and various aspects of stimulus motion are obtained at high temporal resolution. These correlations provide a detailed description of the temporal dynamics of, for example, direction tuning and velocity tuning. In addition, with a spatial array of independently moving RPAs, the MRC method can be used to measure spatial as well as temporal receptive field properties. We demonstrate that MRC serves as a powerful and time-efficient tool for quantifying receptive field properties of motion selective cells that yields temporal information that cannot be derived from existing methods.

© 2002 Elsevier Science B.V. All rights reserved.

Keywords: Motion vision; Reverse correlation; Direction selectivity; Visual cortex; Area MT; Cat; Monkey

1. Introduction

The introduction of white noise stimuli and triggered averaging in neuroscientific research (de Boer and Kuypers, 1968) provided new and important insights in response properties of neurons throughout the nervous system. Examples of systems in which this method was used are cat primary auditory cortex (van Gisbergen et al., 1975; Jenison et al., 2001), cat primary visual cortex (Citron et al., 1981; Jones and Palmer, 1987; Eckhorn et al., 1993; DeAngelis et al., 1995; De Valois et al., 2000), catfish retina (Hida and Naka, 1982), human motor units (Farina et al., 2002), monkey visual area MT (Livingstone et al., 2001; Bair et al., 2002) and fly H1 cells (Srinivasan et al., 1993; Haag and Borst, 1997).

In visual system research, reverse correlation is an effective tool for studying linear response characteristics of single neurons. Stimuli typically consist of spatial patterns, of which luminance contrast of constituting elements is modulated according to a pseudo random sequence. The spike triggered average stimulus is proportional to the first order Wiener kernel and provides the best linear approximation of the cell's spatio-temporal impulse response.

In principal, a motion impulse response can be derived by investigating higher order kernels (Marmarelis and Naka, 1973; Citron and Emerson, 1983; Livingstone et al., 2001). Motion energy in a spatio-temporally uncorrelated stimulus is sparse however, which results in either low signal to noise ratios or time-consuming recordings. We propose to surpass these constraints by measuring the motion impulse response directly with a subspace reverse correlation technique (Ringach et al., 1997a). Instead of random luminance contrast modulation, this requires a stimulus in which random motion impulses are presented. We

* Corresponding author. Tel.: +31-30-2533-673; fax: +31-30-2542-219.

E-mail address: b.g.borghuis@bio.uu.nl (B.G. Borghuis).

developed a paradigm that satisfies this constraint. We call it motion reverse correlation (MRC).

In an MRC experiment, the visual system is stimulated with motion impulses by presenting a rapid sequence of displacements of a random pixel array (RPA; Julesz, 1971). Parameters for each displacement are drawn randomly from a predefined set. Cross-correlating the response of a motion sensitive neuron with the motion impulse sequence yields a receptive field reconstruction in the motion domain. This is a description of the temporal dynamics of motion selectivity, from which we can derive the cell's motion tuning curves over time.

Receptive field properties of motion selective cells are traditionally quantified by measuring the response to sustained motion stimuli, presented in consecutive trials of multiple second durations (further referred to as the 'classic' method). This constitutes the cell's 'step response' to the motion stimulus and provides tuning functions for various motion parameters. The step response however, reflects both the underlying impulse response and motion integration over time. The MRC method accurately and efficiently measures the 'motion impulse response'. The highly interleaved MRC stimulus makes measurements relatively robust to fluctuations in responsivity and does not induce adaptation to strong or prolonged stimuli (Chichilnisky, 2001). The statistical independence of subsequent directions of motion is an essential difference between the MRC paradigm and the 'continuous mapping' method (Schoppmann and Hoffmann, 1976; Treue et al., 2000) that also employs continuously changing directions of motion but is highly correlated over time, which excludes the possibility of computing reverse correlograms with a high temporal resolution.

In the present study, we illustrate the potential of the MRC-paradigm by applying it to the analysis of complex cells in cortical areas 18 and PMLS of anesthetized cats and single units in area MT of an awake, fixating monkey. We compare tuning functions measured with the MRC method to results obtained from the same cells with the classic method and find that the results are highly similar. We show how MRC additionally yields a detailed description of the temporal dynamics of direction and velocity tuning.

A straightforward extension of the method is used to measure spatial receptive field structure of directionally selective cells, elucidating the temporal dynamics of center-surround interactions in macaque area MT. The use of spatial motion white noise for mapping receptive field structure has been previously described by Srinivasan et al. (1993). The method they describe yields a vector weighted motion receptive field map that is formally identical to that obtained with MRC. The MRC method however, due to its computational basis, i.e. reverse correlation, adds a temporal dimension to

the receptive field measurement. This is an essential difference and as a result, the MRC method enables the study of both spatial and temporal interactions, at high temporal resolution.

In summary, MRC quantifies aspects of the motion receptive field, such as the temporal dynamics of motion selectivity and the time course of specific stimulus interactions, that cannot be derived from experiments in which continuous motion is presented. Furthermore, due to its efficiency, there are few limitations to the subspace of motion parameters included in an experiment. This opens the door to new experiments that will provide novel insights into cortical processing of visual motion.

2. The MRC method

The visual stimulus consists of a rapid sequence of displacements of a random pixel array (RPA). The RPA is displaced according to parameters chosen at random from a predefined set. Elements in this set will be referred to as 'states'. Each state occurs with equal probability and defines the step size, delay and direction of the displacement, as well as additional parameters, such as luminance-contrast and pixel size. States in a single experiment may differ in one aspect, such as direction of motion in a direction-tuning experiment or in multiple aspects. The RPA makes a single step during each state before the next randomly chosen state starts.

We compute the temporal dynamics of motion tuning by reverse correlating a cell's responses with the motion impulse sequence. Reverse correlograms for the different states are computed separately. For each spike, the relative time of occurrence of motion impulses from the different states is added to a corresponding array. Fig. 1 illustrates the procedure for computing the reverse correlation function of motion in the upward direction. Reverse correlograms are normalized by dividing the number of motion impulses in each 0.5 ms time bin of the different cross correlation functions, by the sum of motion impulses in the bins. Values now range from 0 to 1 and zero-correlation level is $1/n$, where n is the total number of states. Correlation functions obtained in this manner express the probability of observing a specific motion impulse at a specific point in time preceding a spike, relative to the probability of observing motion impulses from any of the other states.

The time of occurrence of spikes and motion impulses is measured at a temporal resolution of 0.5 ms. This results in a sparse distribution of motion impulses and therefore in a somewhat noisy cross correlation function, depending on the actual total number of spikes. The cross correlation function can be improved easily however, without significant loss of information. Fig. 2 shows the effect of smoothing a motion reverse correlo-

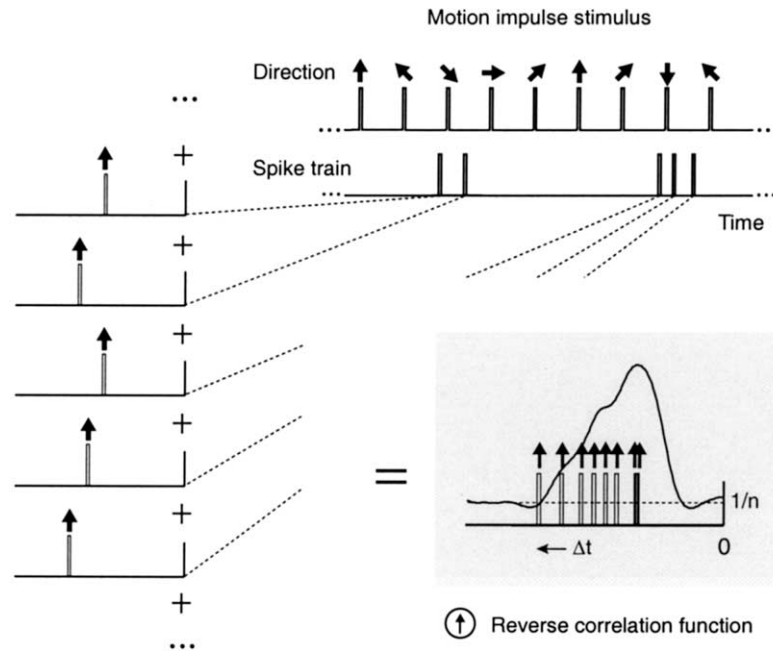


Fig. 1. Computation of the motion reverse correlogram for direction tuning. The neural response is cross correlated with the motion impulse sequence. Motion impulses from different directions are sorted into different arrays. This way, a series of reverse correlograms is obtained, one for each direction of motion. The example illustrates the computation of the reverse correlogram for motion in the upward direction. Motion impulses are added to an array at their specific time of occurrence relative to each spike. Reverse correlograms are subsequently normalized by dividing the number of motion impulses in each 0.5 ms time bin of the different cross correlation functions, by the sum of motion impulses for different directions. Values now range from 0 to 1 and zero-correlation level is $1/n$, where n is the total number of directions. Correlation functions obtained in this manner express the probability of observing a specific motion impulse at a specific point in time preceding a spike, relative to the probability of observing motion impulses from any of the other directions.

gram by sliding window averaging with a Gaussian profile of different widths (S.D.). For the results presented in the remainder of this article, we use a S.D. of 5 ms as this removes most of the noise without affecting the shape of the function and its main parameters. The temporal position of its optimum and the first and last point of significant deviation from chance level correlation remain unaltered (Fig. 2).

Significance levels for the reverse correlograms are derived from the mean and variance of the non-correlated part of the correlation function (Mazer et al., 2002). For this we use a time interval in the smoothed reverse correlogram *after* the spike, as correlations between spikes and stimuli that have not yet been presented must be interpreted as chance level correlations.

Pseudo-random sequences are generated by randomly shuffling an array containing equal numbers of elements referring to each of the states. This ensures that at the end of the measurement, each state has occurred equally often, yet in a pseudo-random order. The length of the sequence and the delay between subsequent steps determine the total duration of an experiment. The length required for obtaining acceptable signal to noise ratios depends on the responsivity of the cell and increases with the number of different states in the MRC-stimulus.

Stimuli were computer-generated (ATI Rage graphics card, Apple Macintosh G4 computer, custom-made software) and displayed on a linearized 19", 100 Hz CRT monitor (400PS, Sony Trinitron) (cat data), or a linearized 21", 75–120 Hz CRT monitor (500PS, Sony Trinitron) (monkey data). Mean luminance was 60.4 cd m^{-2} . We used a square or rectangular aperture ($100\text{--}400 \text{ deg}^2$) centered on the receptive field of the cell under study and positioned at 57 cm from the optic node.

The RPA ($200 \times 200\text{--}600 \times 600$ pixels) is copied at frame rate (75–120 Hz) from a source bitmap image (7000×7000 pixels). Dot pattern of the source image remains unaltered throughout the measurement. Specific measures were taken to prevent the 'random walk' of the RPA from exceeding the boundaries of the bitmap. Copies of the top and left flanks were added to the right and bottom, respectively and corner patterns were identical (Fig. 3). Upon reaching the edge, the RPA was shifted to the opposite side of the source bitmap, prior to its next displacement.

We present results obtained from different MRC experiments, in areas 18 and PMLS of anesthetized cats and area MT of an awake, fixating macaque monkey. In the first experiment, we measure the temporal dynamics of direction tuning (eight states, $0\text{--}315^\circ$). Pixel size of the RPA was optimized for the cell under study. The time-interval and magnitude of the

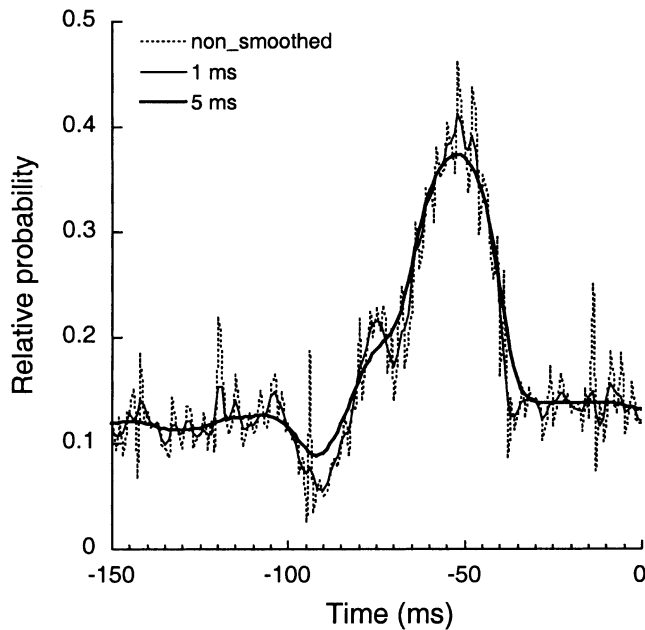


Fig. 2. Smoothing the motion reverse correlogram with a sliding Gaussian window. Example from a single unit in monkey area MT. Temporal resolution of the impulse sequence and spike train is 0.5 ms. The RPA is typically displaced every 20 ms. As a result, the motion impulse sequence is sparse, which, depending on the total number of spikes in the response, leads to noise in the reverse correlograms. Dotted line represents a typical motion reverse correlogram prior to smoothing. To remove high frequency noise, the function was smoothed by sliding averaging with a Gaussian window with a S.D. of 1 ms (thin line) and 5 ms (thick line). The latter removes most of the noise without significant loss of temporal resolution. The global shape of the curve, its maximum and optimum, remain unaffected.

displacements were set to match the preferred delay and step size of the cell measured with classic methods. In the second experiment, we measured the temporal dynamics of velocity tuning in macaque area MT. The stimulus consists of 12 states: six different step sizes ($0.025\text{--}0.8^\circ$ per step) in both preferred and anti-preferred direction. Anti-preferred motion states are added to determine directional selectivity at each velocity. In addition, it prevents adaptation of the cell to continuous motion in the preferred direction.

We compare the reverse correlation results to tuning curves measured with a classic stimulus paradigm, consisting of drifting RPAs identical to the reverse correlation stimulus in contrast and pixel size, but moving continuously in consecutive 2 and 1 s trials (cat and monkey, respectively). Tuning curves are compared on the basis of the mean and σ of a Gaussian fitted to the tuning curves (least squares fit in Matlab). These two parameters reflect the cells' preferred direction and tuning width, respectively.

We extend our investigation by measuring spatio-temporal interactions with a modified version of the MRC stimulus. Spatial receptive field structure of area MT neurons was measured with a spatial

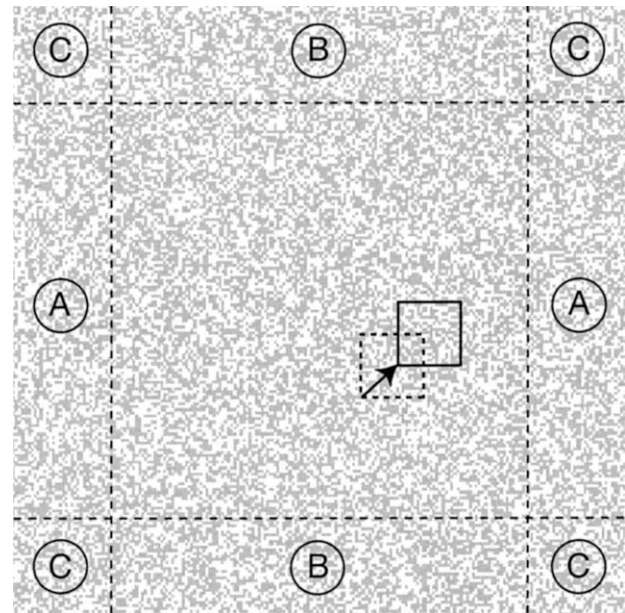


Fig. 3. Motion reverse correlation stimulus. Motion impulses are generated by displacing a random pixel array (RPA). The RPA is displaced according to a pseudo-random sequence, specifying step size, delay and direction of the displacement. The RPA is copied at frame rate from a predefined source bitmap image. Dashed and solid rectangles illustrate the presented fraction of the image on the screen before and after a motion step. Care must be taken to prevent the 'random walk' of the RPA from crossing the borders of the map. This is specifically important at large step sizes and with long random sequences. We avoided this problem by adding a copy of the left flank of the image to the right flank, top flank to the bottom and by making the corner patterns identical. During the experiment, the RPA is shifted to the opposite side of the map upon reaching a border. This effectively turns the bitmap into a torus, allowing for unlimited sequence lengths, even at high velocities.

array of RPAs, e.g. 5×5 and even 10×10 RPAs (further referred to as 'patches') in a square, seamless grid. All patches are displaced simultaneously in their own section of the grid, each one according to its own unique pseudo-random sequence. A spike-triggered average is computed for each patch in the grid by reverse correlating the neural response with the motion impulse sequence. Examples of the stimuli used in this study can be viewed at our website (<http://www-vf.bio.uu.nl/lab/NE/publications/BB/MRC/methods.html>).

2.1. Electrophysiological methods

Data were obtained from single cells in areas 18 and PMLS of anesthetized adult cats (both males and females, 3–5 kg) and area MT of an awake fixating macaque monkey. Preparatory procedures were standard and in accordance with the guidelines of the Law on Animal Research of the Netherlands and of the Utrecht University's Animal Care and Use Committee.

2.2. Cat

Anesthesia was induced by ketamine hydrochloride injection (Aescoket-plus, 20 mg kg⁻¹, i.m.) and maintained by artificial ventilation with a mixture of 70% N₂O–30% O₂ and halothane (Halothaan, 0.4–0.7%). To minimize eye movements, muscle paralysis was induced and maintained throughout the experiment by infusion of pancuronium bromide (Pavulon, 0.1 mg kg⁻¹ h⁻¹, i.v.).

Extracellular single unit recordings were obtained with tungsten microelectrodes (TM33B20KT, World Precision Instruments, USA, typical impedance 2.0 MΩ) at Horsely–Clark coordinates 0–7 mm posterior, 0–7 mm lateral (Reinoso-Suarez, 1961). Action potentials from single cells were detected with a window discriminator (BAK Electronics Inc., USA) and their time of occurrence sampled at 2.0 kHz (NI-DAQ PCI 1200, National Instruments, USA) for on-line analysis and storage (Apple Macintosh G4 computer, custom-made software). Oxygen-permeable contact lenses (+3.5 to +5 diopters, courtesy of NKL, Emmen, Holland) were used to both focus the visual stimulus on the retina and protect the *corneae*.

2.3. Monkey

One adult male rhesus macaque (*Macaca mulatta*) was used in this study. The monkey was implanted with a head holding device, a search coil for measuring eye movements (Judge et al., 1980) and a stainless steel recording cylinder placed over a craniotomy above the occipital lobe. The animal was trained to maintain fixation on a small spot (0.5°) on a computer screen at 57 cm. The monkey's eye position was measured using a scleral search coil system. Eye movement recordings were sampled at 500 Hz.

The monkey was rewarded for correct fixation during the recording with a drop of water or juice, delivered at 3.5 s intervals. Correct fixation was defined as having the monkey fixate within a circular 1° radius around the fixation dot. At this window size, eye blinks normally lead to fixation breaks. Upon breaking fixation, the stimulus and fixation dot disappeared for 0.5 s, which served as negative feedback for the animal. The fixation dot subsequently reappeared and after 0.2 s of correct fixation, the stimulus continued. It has been shown that fixational eye movements over a textured surface may influence the response of neurons in area MT (Bair and O'Keefe, 1998). The MRC stimulus presents RPA motion in rapidly changing directions (20 ms intervals). This is unlikely to evoke correlated fixational eye movements at the time scale of the reverse correlation measurements. The MRC stimulus therefore minimizes effects from residual eye movements.

During experimental sessions, a stainless steel guide tube was used to penetrate the dura. A plastic grid inside the cylinder with holes at 1-mm intervals provided a coordinate system of guide tube positions at different penetrations. A parylene insulated Tungsten microelectrode (1–2 MΩ at 1 kHz; Microprobe Inc.) was inserted manually through the guide tube and then manipulated by an MC-4B micropositioning controller (National Aperture Inc.). Area MT was identified by its anatomical location including the recording depth, the transition between gray matter, white matter and sulci along the electrode track and by its electrophysiological properties, a.o. the prevalence of direction selective units, the similar direction tuning of nearby single or multi-unit recordings, the receptive field size according to eccentricity and the changing direction tuning along the electrode track. We have no histological confirmation of the recording sites because the monkey is currently used in other experiments.

3. Application of the MRC method

3.1. Direction and velocity tuning

The MRC stimulus is effective in evoking directionally selective responses from cells in the visual cortex. The ratio of spike count and the total number of motion impulses during direction tuning measurements was on average 1.00 (±0.91), 0.24 (±0.26) and 0.38 (±0.36) for complex cells in cat area 18 ($n=81$), area PMLS ($n=28$) and macaque area MT ($n=92$), respectively. Although the responsivity of cells varies widely, highly significant reverse correlograms were obtained from cells throughout the entire range.

In anesthetized cats, MRC experiments with a single RPA have a typical duration of 5000–20 000 × 20 ms = ±1.5–7 min. In area MT of an awake macaque monkey, ≈3 min is required to present an entire sequence of 5000 states, due to the monkey breaking fixation every 10–15 s. Artefactual effects from breaking fixation are avoided by repeating the stimulus sequence preceding the break by one period of the reverse correlogram (typically 200–300 ms) after correct fixation is regained. Spikes fired during this period are excluded from the analysis.

Fig. 4 shows results from a directional MRC experiment. Data were obtained from motion selective cells in an anesthetized cat and an awake, fixating macaque monkey. Top panels (Fig. 4A, B) show the reverse correlograms after sliding window averaging with a Gaussian profile ($\sigma=5$ ms). The eight lines represent the reverse correlation functions for the different directions of RPA-motion (0–315°). Each line represents the chance that, at a particular point in time preceding the spike, a motion impulse in that specific direction

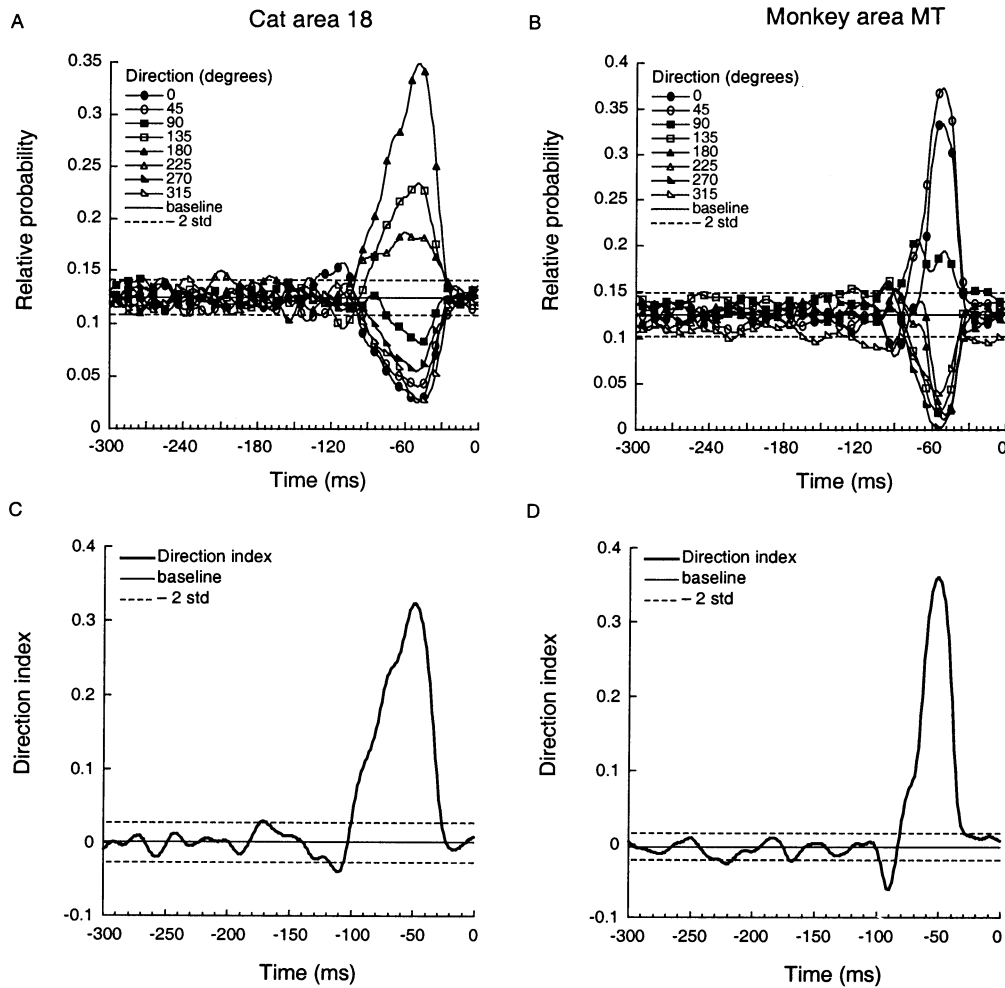


Fig. 4. Direction tuning reverse correlograms. The motion reverse correlation stimulus consisted of eight states moving the RPA in different directions (0–315°). (A) Reverse correlogram obtained from a single neuron in cat area 18 based on the response to 10 000 motion impulses. Motion impulses were delivered with 40 ms intervals. Some 5222 spikes were fired throughout the stimulus presentation. A strong correlation is observed between spikes and motion in the leftward direction (180°, closed triangles) around $t = -50$ ms. (B) Reverse correlogram obtained from a single unit in area MT of an awake, fixating monkey. Motion impulse sequence-length was 15 000. In this measurement, motion impulses were delivered with 20 ms intervals. Total spike count during the recording was 7263. This cell shows a preference for motion in the upper-rightward direction (45°, open circles). In both examples, we find strong negative correlation with motion in the opposite or anti-preferred direction. (C, D) Direction tuning indices computed from the reverse correlograms shown in (A) and (B), respectively. The direction index is defined as the difference between the relative probabilities for observing the preferred and the anti-preferred direction. Baseline and S.D. are obtained from the non-correlated part of the reverse correlation function (see Section 2).

occurred. Both examples show highly significant correlations between particular directions of motion and the occurrence of spikes. Correlations over time are expressed as the relative probability that a motion impulse in a particular direction occurred, given a spike at $t = 0$. In Fig. 4(C, D) the time course of direction selectivity is plotted (for definition see the legends).

To verify the MRC results, we also measured responses of single neurons stimulated with a large-field RPA drifting in one of eight directions in consecutive, 2 and 1 s trials (cat and monkey, respectively, marked 'classic' in Fig. 5). Examples of tuning curves obtained with the two different methods are presented in Fig. 5(A, B). Clearly, the cells' preferred directions and

tuning width measured with the two different methods correspond well.

We quantified the similarity of direction tuning characteristics measured with the two methods over a pool of cells (cat: $n = 27$; monkey: $n = 13$). To this end, Gaussian functions were fitted to both tuning curves. Mean and σ of the Gaussian fits reflect the measured preferred direction and direction tuning width, respectively. Only those cells for which the classic tuning curve could be fitted satisfactorily (fit-error < 15%) with a Gauss function were included in the analysis. Fit-errors were computed as the mean absolute difference, normalized to the maximum of the measured tuning curve:

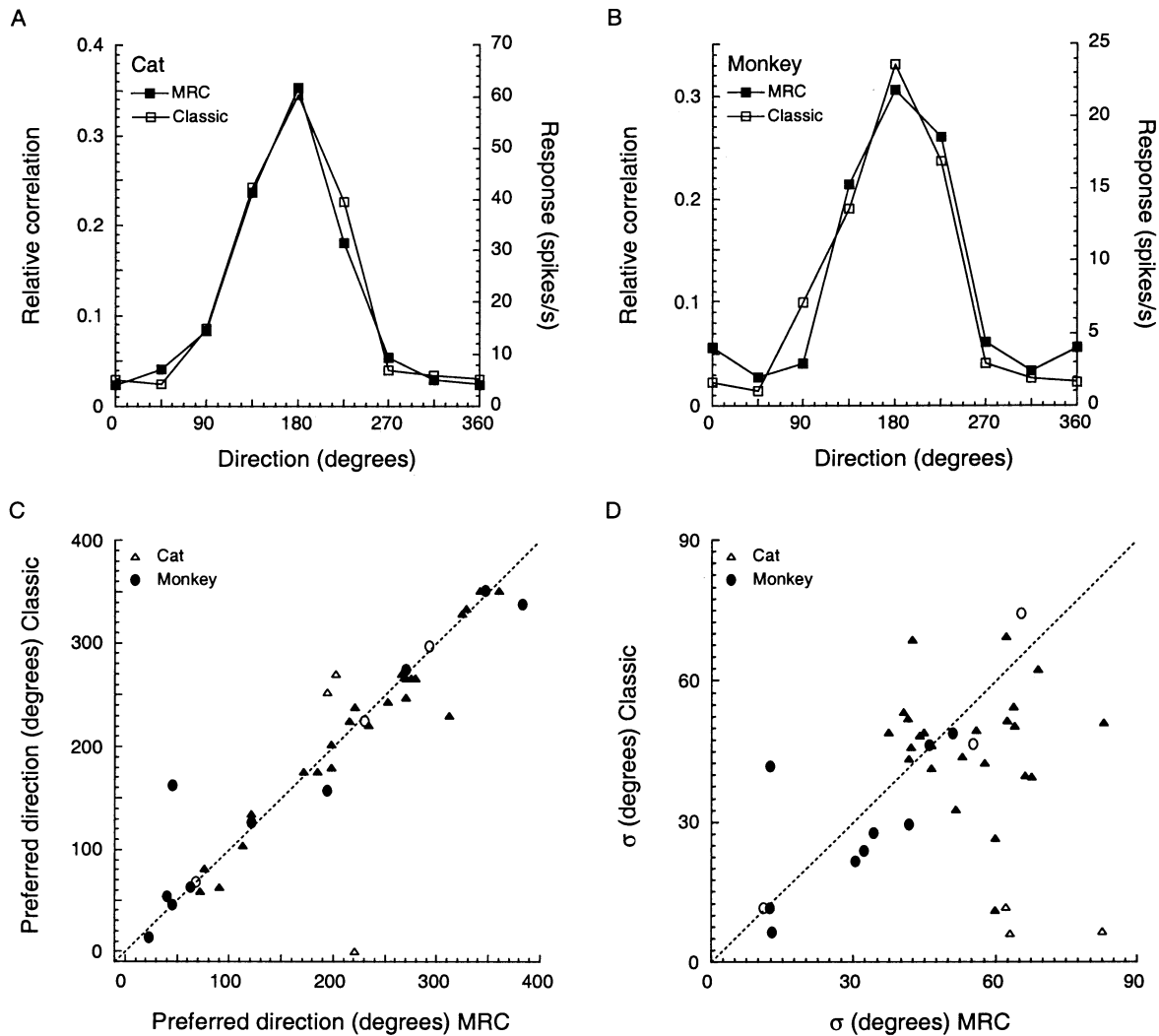


Fig. 5. Comparing direction tuning curves obtained with continuous motion (1-s trials) and MRC method. The continuous motion paradigm will be referred to as 'classic'. Direction tuning curves were obtained from single units in area 18 and PMLS of anesthetized cats ($n = 27$) and area MT of an awake macaque monkey ($n = 13$). Examples of results obtained with the two methods are shown in panels (A) and (B). For each cell, we compared the mean and σ of a Gaussian fitted to the classic (open squares) and MRC (solid squares) direction tuning curves. Mean and σ of the fit reflect the cell's preferred direction and the broadness of its direction tuning, respectively. Scatter plots comparing mean and σ obtained from classic and MRC measurements are shown in panels (C) and (D). For three cells in the cat and three cells in MT (open symbols), tuning curves measured with the classic method could not be fitted satisfactorily with a Gaussian function (fit error $> 15\%$).

$$E = \frac{100}{m} \sum_{(i=1)}^m \frac{|x_i - d_i|}{d_{\max}} \quad (1)$$

where m is the number of directions, x is the value obtained from the Gaussian fit, d is the corresponding measured value and d_{\max} is the peak value of the measured tuning curve. On the basis of the 15% criterion, three classic measurements of cells in cat area 18 and three cells in macaque area MT (open symbols in Fig. 5, panel C and D) were excluded from further analysis. The MRC data obtained from these cells however, are used in Fig. 6.

Similarity of mean and σ values was assessed with a paired t -test. Both cat and monkey data show no

significant difference between the preferred directions measured with the classic and MRC method (cat: $P = 0.34$, $n = 24$; monkey: $P = 0.70$, $n = 10$). For area 18 and PMLS cells, we find a small difference in measured σ (7.4° , $P = 0.048$, $n = 24$). Data from macaque area MT shows no significant difference in the measured tuning widths ($P = 0.50$, $n = 10$).

A histogram of tuning widths measured with the MRC method in cat and monkey, is shown in Fig. 6. Average tuning width over the population of single units in macaque area MT was $39.9 \pm 15.7^\circ$ ($n = 92$). Measurements obtained from cat area 18 and PMLS yield an average tuning width of $55.9 \pm 12.4^\circ$ ($n = 27$). These values are in agreement with average tuning widths in

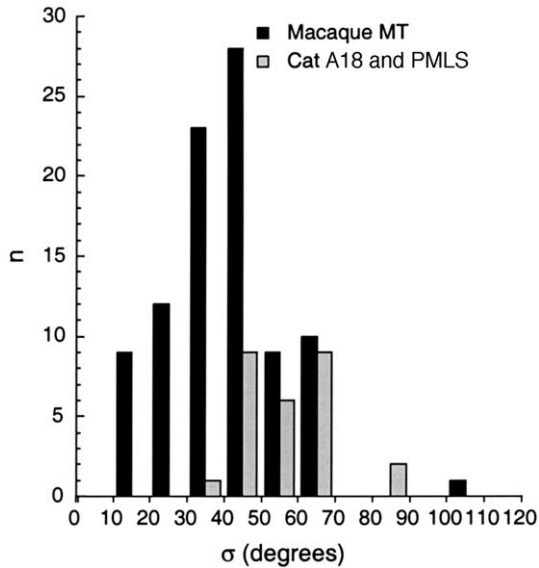


Fig. 6. Distribution of tuning widths measured with the MRC method. Tuning width is expressed as the S.D. (σ of a Gauss function fitted to the direction tuning curve). Full width at half height of the tuning curve therefore corresponds to 2σ . Average tuning width over the population of single units in macaque area MT was $39.9 \pm 15.7^\circ$ ($n = 92$). Measurements obtained from cat area 18 and PMLS yield an average tuning width of $55.9 \pm 12.4^\circ$ ($n = 27$).

area MT reported elsewhere (Albright, 1984; Snowden et al., 1992; Lagae et al., 1993; Britten and Newsome, 1998).

In addition to providing the same information as the continuous motion paradigm, MRC has the important advantage that a high resolution temporal dimension is added to the measurement. Therefore, the temporal development of directional selectivity can be examined as a function of time. A polar plot movie, showing the temporal dynamics of direction tuning for a cat area 18 cell can be viewed at our web-site (<http://www-vf.bio.uu.nl/lab/NE/publications/BB/MRC/fig5d.html>).

To measure velocity tuning, we defined a stimulus consisting of states differing in both direction of motion and step size, i.e. the magnitude of the displacement of the RPA. We show two examples obtained from macaque area MT (Fig. 7). In both experiments, 12 states were used, i.e. six different velocities, in both the preferred and anti-preferred direction. Data analysis is the same as described for the direction tuning experiment and provides a description of the temporal dynamics of velocity tuning (data not shown). We find that the tuning curves measured with the MRC method are similar to those obtained with the classic, sustained motion paradigm. The methods yield similar tuning curves and corresponding values for the cells' preferred velocity.

3.2. Number of states and sequence length

The effect of increasing the number of states in an MRC direction tuning experiment was investigated with MRC stimuli consisting of radially symmetrical sets of four, eight and 16 directions (Fig. 8). MRC tuning curves express the relative probability for observing a particular motion direction present in the stimulus. Thus, the probability for each individual direction scales with the total numbers of states. Tuning curves were therefore normalized by multiplying the relative probability for each direction with the total number of directions in the stimulus. For comparison, direction tuning parameters of the measurements preferred direction and tuning width were obtained from a Gaussian fit.

For two cells, direction tuning curves were obtained with four, eight and 16 directions present in the stimulus. Preferred directions computed from the three measurements (four, eight and 16 directions) were 63.0 , 58.5 and 63.0° (Fig. 8, left panel) and 0 , 13.5 and 11.3° , respectively (Fig. 8, right panel). Corresponding σ values of the fits were 28.4 , 26.7 and 31.7° and 47.9 , 31.1 and 23.7° . Part of the difference observed for the four-direction condition may be a result of fitting four data points with a Gauss function and therefore reflect sampling errors.

We proceeded by investigating the number of motion impulses required to obtain a reasonable estimate of a cell's direction tuning curve. To this end, tuning curves obtained from fractions of the motion impulse sequence were compared with a Gaussian function that was fitted to the tuning curve obtained from the entire sequence (eight directions, 5000 motion impulses, example shown in Fig. 9A). Deviations between the two curves were assessed with Eq. (1). As the sequence can be divided into many short fragments (e.g. 500 fragments of ten impulses each), multiple error values can be obtained for each fragment length. We exploited this possibility by computing errors from a maximum of 30 non-overlapping fragments, which were subsequently averaged. Solid circles show the results obtained from the ten MT neurons from which we have measured both with the classic and the MRC method.

Results obtained from area MT are shown in Fig. 9(B). The effect of the number of motion impulses on the quality of the estimated tuning function resembles an exponential decaying function (solid circles). Speed and accuracy of the MRC method expressed in this manner allow a direct comparison to the average results obtained with the classic method (open squares). Classic measurements consisted of nine stimuli, i.e. eight motion directions and one 'blank' stimulus. Stimuli had a duration of 1 s and the inter-stimulus interval was 0.13 s. The minimal time required for a single presentation of the stimuli was therefore 10.2 s. We find that with the

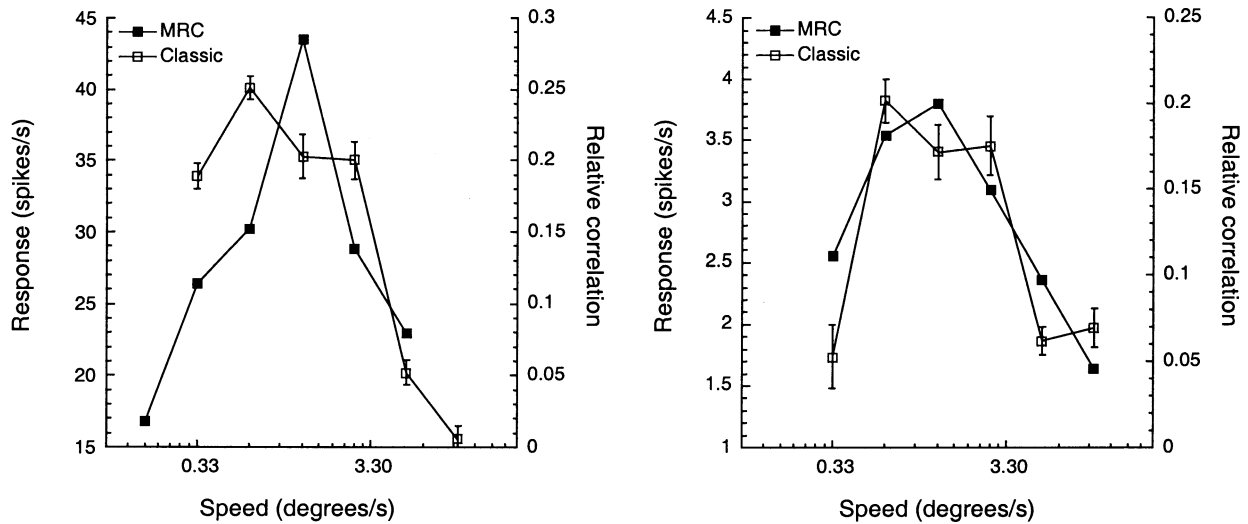


Fig. 7. Velocity tuning curves measured in area MT. Panels show examples from two single units in area MT of an awake, fixating monkey. Tuning curves marked 'classic' (open squares) were obtained with random pixel arrays drifting at different velocities in the preferred direction. Stimuli were presented in random interleaved 1-s trials. Each trial was repeated ten times, error bars indicate S.E.M. values. MRC velocity tuning curves (solid squares) were obtained with a motion impulse sequence consisting of six velocities in both the preferred and non-preferred direction. Units of the MRC data (relative correlation) cannot be compared directly to those of the classic method (spikes per second). The two methods however, yield similar preferred velocities and comparable velocity tuning curves.

stimulus parameters used here (delay 20 ms, state duration 20 ms), the fit error is $< 10\%$ within ≈ 15 s. This is substantially faster than the classic method. The fit error decreases with increasing time. After 2 min (13 repeats of the classic method), the deviation from the fitted Gauss function is approximately twice as large as

that of the MRC measurements (7.65 and 3.83%, respectively). Note that this comparison is based on measurements from the same cells ($n = 10$). MRC results averaged over 88 MT cells (gray lines) show that the MRC results from this subpopulation are typical for the cells that we recorded.

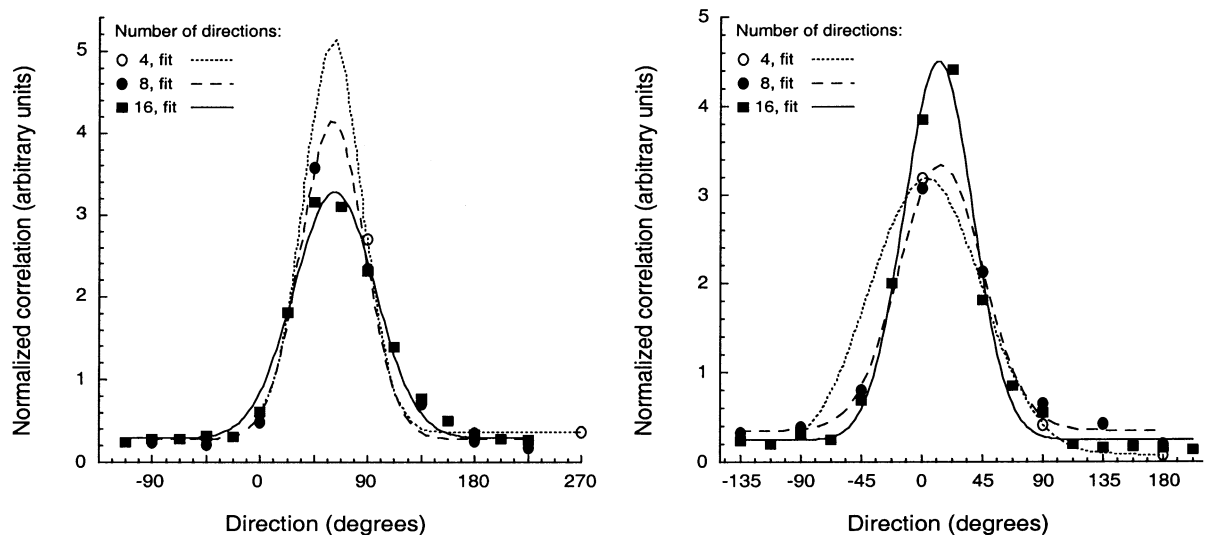


Fig. 8. Direction tuning measured with varying numbers of directions. Panels show examples of direction tuning curves obtained with the MRC method in area MT of an awake macaque monkey. Direction tuning curves were measured with a MRC stimulus consisting of motion impulses in four, eight or 16 directions, evenly distributed over 360° . Because absolute probabilities are inversely proportional to the number of directions in the stimulus, tuning curves for the different numbers of directions were normalized by multiplying the relative probabilities with the number of directions that were presented. To assess the effect of increasing numbers of directions on the estimated tuning characteristics of the cells (preferred direction and tuning width), Gauss functions were fitted to the three data sets obtained from each cell. Preferred directions estimated from the four, eight and 16 direction measurements were 63.0 , 58.5 and 63.0° (left panel) and 0 , 13.5 and 11.3° , respectively (right panel). Corresponding σ values of the fits were 28.4 , 26.7 and 31.7° and 47.9 , 31.1 and 23.7° , respectively.

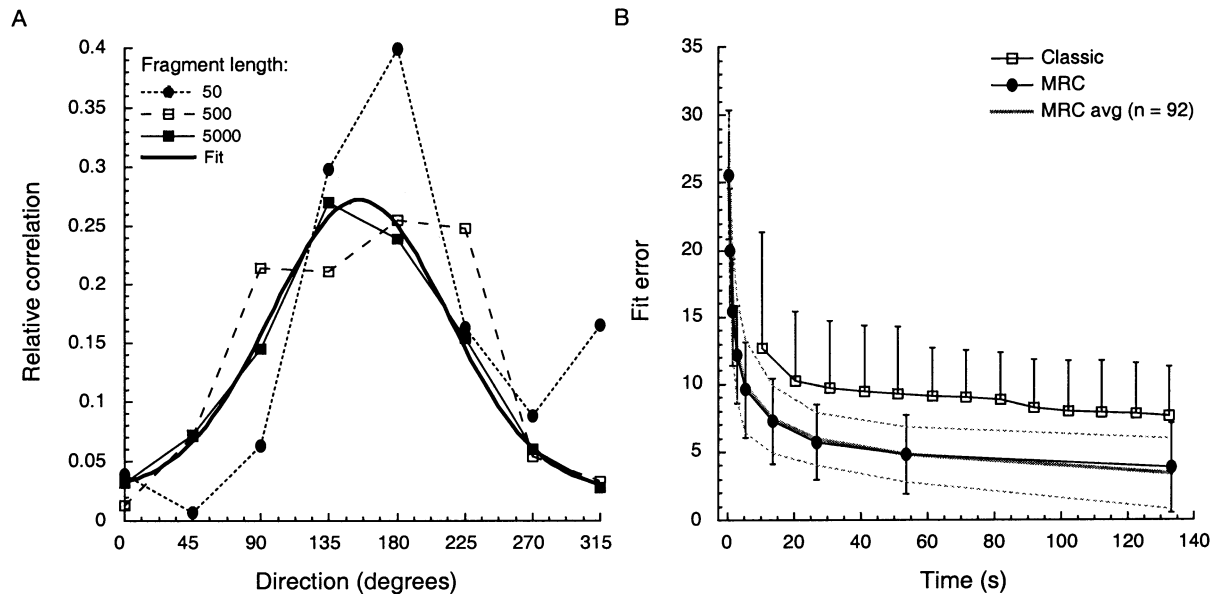


Fig. 9. Improvement of direction tuning curves with increasing sequence length. The time required to obtain a cell's direction tuning curve was estimated by computing reverse correlograms from the response to increasing numbers of motion impulses (10–5000, data partly shown in panel A). A Gaussian function (thick line) was fitted to the tuning function derived from the response to the entire motion impulse sequence. Deviation between this fit and tuning curves based on different fragment lengths was computed with Eq. (1). During the first seconds of presentation, the quality of the MRC tuning curves improves very rapidly. After ≈ 15 s of stimulus presentation, average deviations are $< 10\%$ and after presentation of the entire motion sequence, error values have decreased to 3.83%. Classic measurements obtained from the same cells are added for comparison (open squares). Throughout the recording, classic measurements yield larger error values. We find only moderate improvement from presenting multiple repeats of the stimuli and after ≈ 2 min (13 repeats), deviations from the Gaussian fit remain approximately twice as large as those of the MRC tuning curves (7.65 and 3.83%, respectively). Average MRC results from 88 MT cells (gray line) ± 1 S.D. (dotted lines) show that the ten cells used in the comparison are representative for the population of MT cells that we recorded.

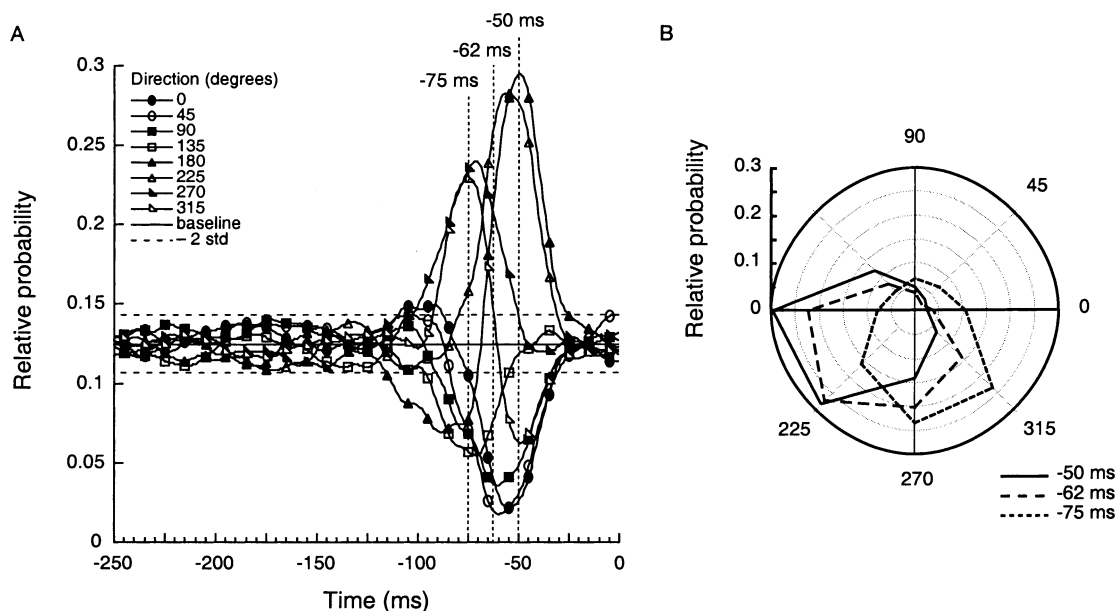


Fig. 10. Temporal offset between peak correlations in a direction tuning experiment. (A) Reverse correlogram obtained from a single unit in macaque area MT. Four directions show a strong positive correlation with the response ($180\text{--}315^\circ$), at different latencies. This is reflected in the polar plot on the right. (B) Polar plots are constructed from the reverse correlograms by taking the probabilities for observing a particular direction of motion at different points in time. Clearly, the cell's preferred direction changes over time.

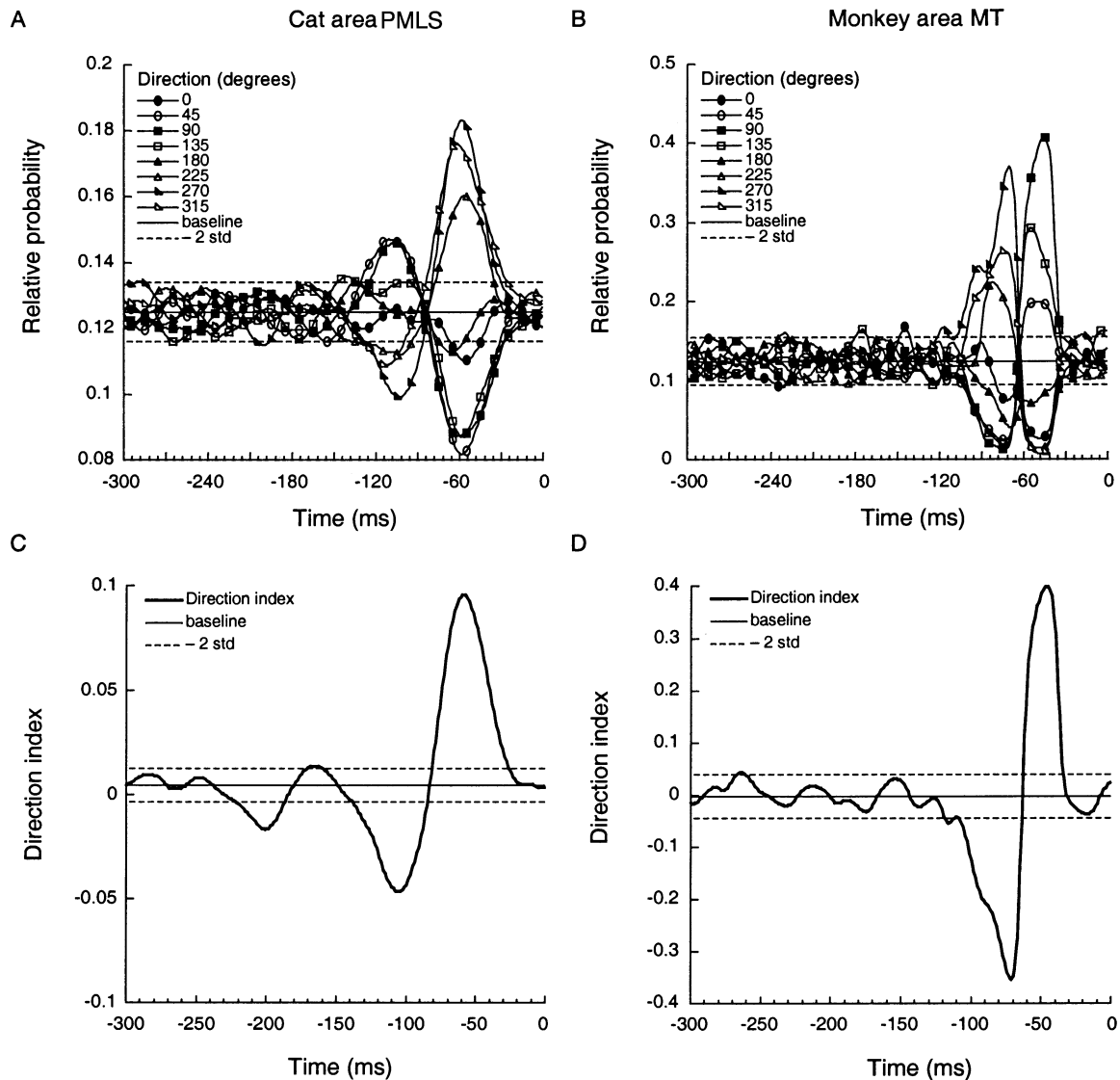


Fig. 11. Biphasic-like behavior. A proportion of the motion selective cells ($\approx 50\%$) in both cat and monkey show two peaks in the reverse correlogram, corresponding to the anti-preferred and preferred direction, respectively. (A) An example from a single unit in cat area PMLS. (B) An example from macaque area MT. Similar response profiles have been found in the luminance contrast domain and are referred to as ‘biphasic’ (e.g. De Valois et al., 2000). The examples shown in Fig. 4 and Fig. 8 resemble a monophasic response. Panels (C) and (D) show the direction index over time computed from the data shown in panel (A) and (B), respectively (see legend Fig. 4 for details).

3.3. Temporal dynamics

We find two phenomena in reverse correlograms obtained from both cat and monkey that illustrate the relevance of investigating the temporal dimension of motion selectivity. First, a proportion of the cells ($\approx 10\%$) show considerable differences in the peak latencies (i.e. time to highest correlation in the reverse correlogram) for different velocities and directions (Fig. 10). This implies that these cells may be stimulated most effectively with a change in velocity or direction of motion, or that different velocities/directions have different response latencies, or both. This resembles the difference between offset and onset latencies re-

ported previously for opposite directions of motion (Bair et al., 2002).

Second, the pool of directionally selective cells forms a bimodal distribution on the basis of their directional reverse correlogram. A proportion of the cells show monophasic behavior, whereas others are biphasic (Fig. 11A, B, respectively). These terms are adopted from luminance-contrast reverse correlograms of LGN cells (e.g. De Valois et al., 2000) and are possibly related to sensitization or fast adaptive processes. This is the first evidence that such a dichotomy exists for directionally selective cells. We are currently further investigating these two phenomena.

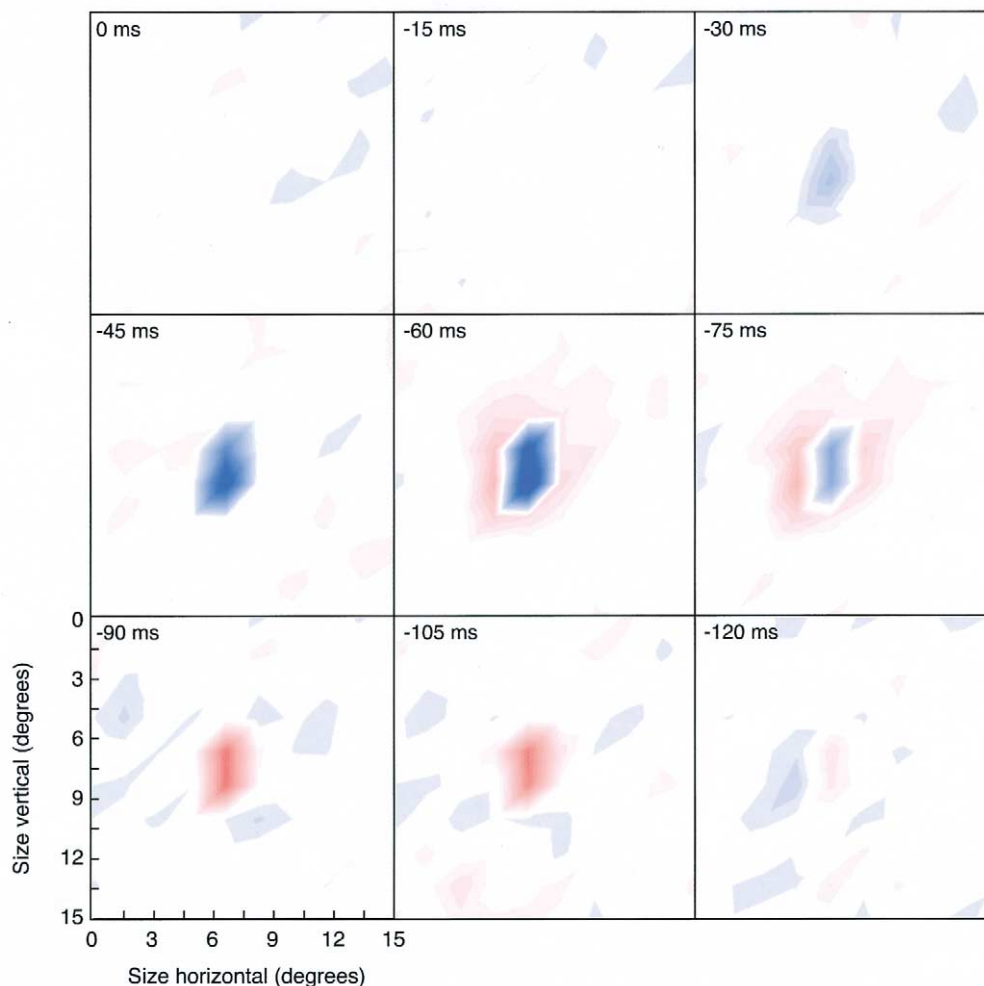


Fig. 12. Spatial receptive field structure. Spatial motion reverse correlograms were obtained with a spatial array of RPAs (dimensions: ten horizontal by ten vertical). Motion impulse sequences from all 100 RPAs were reverse correlated with the neuron's response. The surface plot shows slices through the spatial array of correlation functions at specific points in time relative to the spike. Plots were made in MATLAB and smoothed by cubic spline interpolation. Significant correlations can be observed from $dt = -30$ to -105 ms. First, there is a strong correlation between the response and motion in the preferred direction in the center. This function peaks around -60 ms. Negative correlations with the preferred direction of motion are found at spatial locations directly around the center. Peak latency of this negative correlation is considerably larger than that of the center (-72 and -60 ms, respectively). After reaching its maximum, the correlation function of the center shows a rapid decline into negative correlation values, before returning to chance level correlations around about $dt = -120$ ms.

3.4. Spatio-temporal receptive field structure

In the direction and velocity tuning measurements described in the previous section, temporal dynamics were investigated with a single, large-field RPA. These measurements therefore reflect the cells' tuning properties spatially integrated across the entire receptive field, ignoring the evidence for center-surround organization and lateral inhibition in primate area MT (Raiguel et al., 1995; Xiao et al., 1995, 1997) and spatial interaction within area MT receptive fields (Britten and Heuer, 1999). To measure spatio-temporal tuning, we therefore extended the MRC paradigm and presented independently moving RPAs in multiple patches simultaneously.

Spatial arrays of up to 10×10 RPAs in a square, seamless grid were used to determine the receptive field structure of single area MT neurons. All RPAs were displaced simultaneously in their own section of the grid, each one according to its own unique pseudo-random sequence. Analogous to the checkerboard stimulus in the luminance-contrast domain (DeAngelis et al., 1995), reverse correlation results in a description of the spatio-temporal receptive field properties of the cell. Spatial MRC experiments require slightly more time (≈ 10 min), due to the increased number of possible stimulus configurations.

An example of results obtained with a spatial MRC stimulus is shown in Fig. 12. The surface plot shows the results of a measurement with a 10×10 RPA array

($15 \times 15^\circ$). Sequence length was 15 000 (i.e. ≈ 7 min of presentation) and during the entire presentation, 24 955 spikes were fired. The cell in Fig. 12 shows a positive correlation with the preferred direction of motion in the center, yet at the same time there is significant correlation with motion in the anti-preferred direction in an area directly surrounding the center. A movie clip of the spatial correlogram at our web-site (<http://www.vf.bio.uu.nl/lab/NE/publications/BB/MRC/fig7b.html>) shows that there is a considerable temporal delay between the peak latency of the receptive field center and its inhibitory surround.

4. Discussion

In this paper we show that the motion reverse correlation paradigm provides a powerful tool for investigating response properties of directionally selective cells. The MRC stimulus elicits strong motion selective responses, and direction- and velocity-tuning curves match tuning curves measured with conventional methods. In addition, it provides novel and detailed insights into stimulus interactions and the temporal dynamics of motion tuning. In the ‘multiple-patch’ configuration, it yields detailed descriptions of spatial receptive field structure and it does so without making a priori assumptions about the receptive field or the role of spatial interactions. Furthermore, the simultaneous presentation of localized stimuli makes the method very time efficient. We have shown that the method yields interesting and unexpected results for recordings in visual cortex of both the anesthetized cat and awake, fixating macaque monkey.

In the present study, we correlate spike trains with individual motion impulses. The same procedure can be used to find correlations between spikes and the occurrence of combinations of subsequent motion impulses. For example, in an eight direction MRC experiment, there are 64 possible state-pair combinations and forward or reverse correlation functions can be computed for the spike train and the occurrence of specific sequences of two, or even multiple states. Although the required sequence length scales with the number of possible combinations and the required recording time is increased, potentially interesting interactions may be found and can even be targeted selectively.

The observation that a cell’s preferred direction measured with the MRC stimulus can change over time (Figs. 10 and 11) leads to the interesting suggestion that at least some directionally selective cells in area MT may be tuned to changes in the direction of motion. This is analogous to results obtained in macaque primary visual cortex, which show that preferred orientation in output layer neurons varies over time (Ringach et al., 1997b). These findings are in general agreement with the

observation that visual cortical cells may be better understood as dynamical systems rather than static receptive fields (DeAngelis et al., 1995; Shapley, 1998). The reverse correlation technique that we present here allows one to study such specific temporal aspects of motion receptive fields in great detail.

The motion reverse correlation function expresses the relative probability of observing a particular state of the motion stimulus at any point in time preceding a spike. Therefore, a high probability for one state or a group of states, by definition, decreases the probability for observing any of the other directions. Probabilities below chance level therefore do not necessarily indicate inhibition. Excitation and inhibition are only defined relative to the other states included in the experiment. Inhibition may show up as a significant negative deviation relative to the other states. In experiments where an absolute distinction between excitation and inhibition is critical, one can include null-states (stationary and or dynamic refreshment) in the state-list.

Our results show that the MRC paradigm can be used to investigate the temporal dynamics of directional selectivity and velocity tuning of cortical neurons. The same paradigm can be used to investigate preferred step and delay combinations, preferred pixel size or stimulus contrast. We show that extending the MRC stimulus to multiple RPA-fields in a spatial checkerboard analogue, enables the mapping of spatial receptive field properties of directionally selective neurons. MRC is therefore particularly suitable for the investigation of center-surround receptive field organization of opposing directions of motion and even tuning for complex e.g. rotational or expansive-motion patterns. The fact that little time is required to measure entire multi-dimensional parameter spaces at high temporal resolution makes the method particularly useful in experiments where awake animals are used and recording time is precious.

Acknowledgements

B.G.B. would like to thank Steve Kalik for introducing him to the computational foundations of the reverse correlation paradigm.

References

- Albright TD. Direction and orientation selectivity of neurons in visual area MT of the macaque. *J Neurophysiol* 1984;52:1106–30.
- Bair W, O’Keefe LP. The influence of fixational eye movements on the response of neurons in area MT of the macaque. *Vis Neurosci* 1998;15:779–86.
- Bair W, Cavanaugh JR, Smith MA, Movshon JA. The timing of response onset and offset in macaque visual neurons. *J Neurosci* 2002;22:3189–205.

- Britten KH, Newsome WT. Tuning bandwidths for near-threshold stimuli in area MT. *J Neurophysiol* 1998;80:762–70.
- Britten KH, Heuer HW. Spatial summation in the receptive fields of MT neurons. *J Neurosci* 1999;19:5074–84.
- Chichilnisky EJ. A simple white noise analysis of neuronal light responses. *Network* 2001;12:199–213.
- Citron MC, Emerson RC. White noise analysis of cortical directional selectivity in cat. *Brain Res* 1983;279:271–7.
- Citron MC, Emerson RC, Ide LS. Spatial and temporal receptive-field analysis of the cat's geniculocortical pathway. *Vis Res* 1981;21:385–96.
- de Boer R, Kuyper P. Triggered correlation. *IEEE Trans Biomed Eng* 1968;15:169–79.
- De Valois RL, Cottaris NP, Mahon LE, Elfar SD, Wilson JA. Spatial and temporal receptive fields of geniculate and cortical cells and directional selectivity. *Vis Res* 2000;40:3685–702.
- DeAngelis GC, Ohzawa I, Freeman RD. Receptive-field dynamics in the central visual pathways. *Trends Neurosci* 1995;18:451–8.
- Eckhorn R, Krause F, Nelson JJ. The RF-cinematogram. A cross-correlation technique for mapping several visual receptive fields at once. *Biol Cybern* 1993;69:37–55.
- Farina D, Arendt-Nielsen L, Merletti R, Graven-Nielsen T. Assessment of single motor unit conduction velocity during sustained contractions of the tibialis anterior muscle with advanced spike triggered averaging. *J Neurosci Methods* 2002;115:1–12.
- Haag J, Borst A. Encoding of visual motion information and reliability in spiking and graded potential neurons. *J Neurosci* 1997;17:4809–19.
- Hida E, Naka K. Spatio-temporal visual receptive fields as revealed by spatio-temporal random noise. *Z Naturforsch [C]* 1982;37:1048–9.
- Jenison RL, Schnupp JW, Reale RA, Brugge JF. Auditory space-time receptive field dynamics revealed by spherical white-noise analysis. *J Neurosci* 2001;21:4408–15.
- Jones JP, Palmer LA. The two-dimensional spatial structure of simple receptive fields in cat striate cortex. *J Neurophysiol* 1987;58:1187–211.
- Judge SJ, Richmond BJ, Chu FC. Implantation of magnetic search coils for measurement of eye position: an improved method. *Vis Res* 1980;20:535–8.
- Julesz B. *Foundations of Cyclopean Perception*. Chicago, IL: University of Chicago Press, 1971.
- Lagae L, Raiguel S, Orban GA. Speed and direction selectivity of macaque middle temporal neurons. *J Neurophysiol* 1993;69:19–39.
- Livingstone MS, Pack CC, Born RT. Two-dimensional substructure of MT receptive fields. *Neuron* 2001;30:781–93.
- Marmarelis PZ, Naka KI. Nonlinear analysis and synthesis of receptive-field responses in the catfish retina. 3. Two-input white-noise analysis. *J Neurophysiol* 1973;36:634–48.
- Mazer JA, Vinje WE, McDermott J, Schiller PH, Gallant JL. Spatial frequency and orientation tuning dynamics in area V1. *Proc Natl Acad Sci USA* 2002;99:1645–50.
- Raiguel S, Van Hulle MM, Xiao DK, Marcar VL, Orban GA. Shape and spatial distribution of receptive fields and antagonistic motion surrounds in the middle temporal area (V5) of the macaque. *Eur J Neurosci* 1995;7:2064–82.
- Reinoso-Suarez F. *Topographischer Hirnatlas der Katze*. Translated edition by E. Merck AG, Darmstadt, Germany, T 24, 1961.
- Ringach DL, Sapiro G, Shapley R. A subspace reverse-correlation technique for the study of visual neurons. *Vis Res* 1997a;37:2455–64.
- Ringach DL, Hawken MJ, Shapley R. Dynamics of orientation tuning in macaque primary visual cortex. *Nature* 1997b;387:281–4.
- Schoppmann A, Hoffmann KP. Continuous mapping of direction selectivity in the cat's visual cortex. *Neurosci Lett* 1976;2:177–81.
- Shapley R. Neurobiology. In the mind's eye of the beholder. *Nature* 1998;395:845–6.
- Snowden RJ, Treue S, Andersen RA. The response of neurons in areas V1 and MT of the alert rhesus monkey to moving random dot patterns. *Exp Brain Res* 1992;88:389–400.
- Srinivasan MV, Jin ZF, Stange G, Ibbotson MR. 'Vector white noise': a technique for mapping the motion receptive fields. *Biol Cybern* 1993;68:199–207.
- Treue S, Hol K, Rauber HJ. Seeing multiple directions of motion—physiology and psychophysics. *Nat Neurosci* 2000;3:270–6.
- van Gisbergen JA, Grashuis JL, Johannesma PI, Vendrik AJ. Neurons in the cochlear nucleus investigated with tone and noise stimuli. *Exp Brain Res* 1975;23:387–406.
- Xiao DK, Raiguel S, Marcar V, Koenderink J, Orban GA. Spatial heterogeneity of inhibitory surrounds in the middle temporal visual area. *Proc Natl Acad Sci USA* 1995;92:11303–6.
- Xiao DK, Raiguel S, Marcar V, Orban GA. The spatial distribution of the antagonistic surround of MT/V5 neurons. *Cereb Cortex* 1997;7:662–77.